

SATELLITE—NASA/JPL-CALTECH/MONTANA STATE UNIVERSITY.
BACKGROUND IMAGE—iGRAPHIC/STOCK

Rapid Design of Deployable Antennas for CubeSats

A tool to help designers compare and select antenna topologies.

M. Sakovsky, S. Pellegrino,
and J. Costantine

Digital Object Identifier 10.1109/MAP.2017.2655531
Date of publication: 24 February 2017

A novel methodology for the rapid preliminary design of deployable antennas for CubeSats is proposed in this article. It uses a graphical representation of antenna performance, consisting of a set of plots of different performance metrics against antenna geometry parameters. Coupled electromagnetic and structural design problems are addressed easily, enabling the rapid and direct comparison of different antenna concepts. This approach is demonstrated for a case study at ultrahigh frequency (UHF), comparing the performance of a dipole, a helix, a conical horn, and a conical log spiral (CLS), all based on dual-matrix composite deployable structures. The initial design space of antenna geometries is

reduced by two orders of magnitude to a set of constraint-satisfying designs. A graphical user interface implementing the approach is presented, and the accuracy of the method is briefly addressed.

DEPLOYABLE ANTENNA DESIGN

The recent growth in low-cost access to space through nanosatellites is providing the impetus for increasing the capabilities of these platforms, for example, by increasing the onboard power and downlink rates for applications such as Earth imaging. CubeSats are a very popular platform, available as commercial, off-the-shelf kits in sizes that are in multiples of the 1U unit (a 10-cm cube). The limited size of CubeSats imposes strict volume limitations on all subsystems and particularly on low-frequency antennas, which have to be folded within the satellite body and deployed after the launch. Common choices for CubeSat antennas are monopole/dipole and patch antennas, which are both commercially available. However, these antennas cannot meet the bandwidth and gain requirements imposed by high bit-rate applications.

Ongoing research is addressing this gap by identifying point designs capable of meeting electromagnetic and packaging requirements simultaneously. Many designs have been recommended for deployable helical antennas including the Helios deployable antenna [1]. Several concepts have been proposed for CubeSat parabolic reflectors including the Ultra-Compact Ka-Band Parabolic Deployable Antenna developed at NASA's Jet Propulsion Laboratory [2] and the mesh reflector developed by BDS Phantom Works [3]. A deployable Yagi-Uda antenna has also been suggested [4].

In general, the design of deployable antennas requires the optimization of performance subject to both electromagnetic and structural constraints. The estimation of electromagnetic performance is usually carried out with numerical simulators, such as ANSYS Electronics Desktop [5], CST [6], and FEKO [7]. Designer interfaces, including a catalog of various antenna structures, have been added to several simulation tools, such as the Antenna Magus tool [8], an add-on interface to CST and FEKO, and the ANSYS HFSS Antenna Design Kit [5]. Even with these aids, an electromagnetic performance optimization and a concept comparison must still be carried out manually.

Structural simulations are also necessary, usually carried out with finite element software, such as Abaqus [9]. In the structures and materials community, existing databases of material properties allow mechanical engineers to quickly compare material performance. An example is the CES Selector, which compares materials by graphically representing their performance according to different metrics [10], [11]. No existing tools consider deployment concepts, which is a parameter critical to the present application. Furthermore, considering electromagnetic and structural requirements separately results in many iterations to complete the design.

These gaps are addressed here through a novel methodology for coupled electromagnetic and structural design of deployable antennas, for the specific case of CubeSats. A

technique for the graphical representation of antenna performance as a function of geometry using a set of two-dimensional plots is presented, which allows many antenna concepts to be directly compared. These plots allow designers to quickly narrow down the design space to the antenna geometries that meet all the requirements.

METHODOLOGY

The proposed rapid design methodology consists of the following steps:

- 1) identifying a set of antenna concepts relevant to the particular application of interest
- 2) for each antenna type, identifying one or more structural architectures and packaging schemes
- 3) obtaining, for each antenna concept, design relationships between the geometry of the antenna and the corresponding electromagnetic and structural performance parameters
- 4) generating graphical representations of the design space, through plots of each geometric design parameter versus all performance parameters, including all considered antenna concepts
- 5) searching for a range of geometric design parameters that allows all requirements to be met, for each of the selected antenna concepts.

This methodology is presented for the specific case of antenna types and packaging schemes recommended for CubeSats, but it can be extended beyond this application.

ANTENNA TYPES

The antenna types selected for demonstrating the methodology are schematically shown in Figure 1. The half-wavelength dipole has been selected for performance comparison because it is already a widely used antenna on CubeSats and can be considered as the fundamental antenna. The fixed patch antenna is a nondeployable reference also available commercially. The helical and CLS antennas have been identified as potential concepts for CubeSats in [1], and they exhibit good electromagnetic and structural performance as shown in [12] and [13]. The conical horn and Yagi-Uda antennas have been chosen to represent frequency operation beyond the UHF bands [4].

The space for the antenna design problem is defined here as the set of antenna geometries that result in acceptable electromagnetic operation. The constraints on the design space are written as a function of antenna height, h , and diameter, D . For the half-wavelength dipole, there is a unique design for each wavelength, λ , with the height, h , given by

$$h = \frac{\lambda}{2}. \quad (1)$$

The length of the dipole is referred to here as the dipole height, for consistency with other antenna types.

For the patch antenna, operation as a broad-side radiator requires that

$$\{0.003\lambda < t < 0.05\lambda\} \cap \left\{\frac{\lambda}{3} < h < \frac{\lambda}{2}\right\}, \quad (2)$$

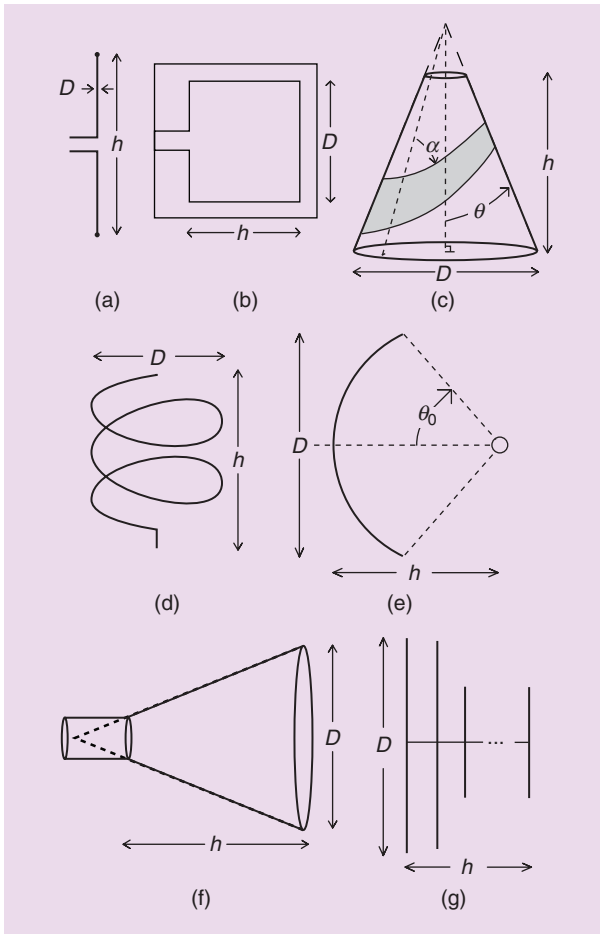


FIGURE 1. The geometry of antennas chosen for the study: (a) dipole, (b) patch, (c) CLS, (d) helix, (e) parabolic reflector, (f) conical horn, and (g) Yagi–Uda.

where t is the patch thickness. Equivalent constraints on D result in a more complex expression.

The constraints for the helix are derived from the desired operation in the endfire mode with circular polarization [14]. The main design parameters are the diameter, conductor pitch, and number of turns of the helix, which can be expressed in terms of the diameter and height

$$\left\{ D = \frac{\lambda}{\pi} \right\} \cap \left\{ \frac{3\lambda}{4} \tan 12^\circ < h < 20\lambda \tan 14^\circ \right\}. \quad (3)$$

Geometries for the conical horn antenna and the parabolic reflector are defined to minimize antenna losses [14]. For the horn,

$$\left\{ \tan 5^\circ < \frac{D}{2h} < \tan 30^\circ \right\} \cap \left\{ h^2 = \left(\frac{D^2}{3\lambda} \right)^2 - \left(\frac{D}{2} \right)^2 \right\}. \quad (4)$$

For the reflector,

$$\{0.65 < \epsilon_{\text{ap}} < 0.80\} \cap \{2\lambda < D < 50\lambda\}, \quad (5)$$

where ϵ_{ap} is the aperture efficiency, used here as explicit constraints on the reflector height are too complex.

For the CLS, there are no explicit equations that define the range of acceptable geometries. Therefore, the experimental data in [15], presented in terms of the cone angle, θ , and wrap angle of the conductors around the cone, α , is used. Typical constraints on these parameters, to achieve a directional radiation pattern, are

$$\{2^\circ < 2\theta < 45^\circ\} \cap \{45^\circ < \alpha < 90^\circ\}. \quad (6)$$

Given θ and α , the upper and lower radii of the cone and its height can then be interpolated from experimental data.

Finally, to achieve a directional radiation pattern, the Yagi–Uda array is typically designed such that [20]

$$\{0.45\lambda < D < 0.49\lambda\} \cap \{0.3\lambda < h < 6\lambda\}. \quad (7)$$

STRUCTURAL ARCHITECTURES AND PACKAGING SCHEMES

Structural architectures that allow efficient packaging exist for all of the aforementioned antennas; most of which are developed specifically for CubeSats. A simple architecture, suitable for the dipole antenna, is a single mechanical hinge supporting a stiff conducting element. The hinge allows the conducting element to be folded parallel to the wall of the CubeSat. A simpler and popular alternative is the metallic tape-spring (i.e., a structure similar to a tape measure) that is elastically bent near the root to fold the rest of the tape spring parallel to the CubeSat, as in [16]. Tape springs can also be used to fold linear arrays such as the Yagi–Uda antennas [18].

A more complex architecture, suitable for the helix antenna, is a cylindrical lattice structure of nonconducting, structural helices connected to conducting helices by scissor joints. This structure behaves as a helical pantograph [13] and therefore has a soft deformation mode that allows axial compaction [Figure 2(a)]. Alternatively, helical conductors can be supported at the base and compacted axially via rotation, resulting in coiling of the conductors around the base, as in [1] and [17] [Figure 2(b)]. Another approach uses dual-matrix composite thin shells made from laminated thin sheets of continuous quartz fibers embedded in two different plastic materials—a stiff epoxy resin and a soft elastomer—that support a set of embedded conducting elements [12]. The regions with soft elastomer matrix form hinge regions arranged according to an origami fold pattern that allows the shells to be folded tightly without damaging the fibers. Compaction in a single direction can be achieved using the Z-folding pattern [Figure 2(c)], and compaction in two directions can be achieved using the Miura–Ori origami pattern.

Parabolic reflector antennas require unique packaging schemes due to the doubly curved surface of the main dish. Typically, these consist of a mesh conductor shaped by supporting curved ribs. The ribs can be rigid with several hinges allowing them to fold alongside a central hub supporting the antenna feed ([Figure 2(d)] [2]). Alternatively, the ribs can be elastic, allowing the mesh to wrap around the central hub using an origami packaging scheme [Figure 2(e)] [3]. Table 1 summarizes the antenna concepts used in the present study.

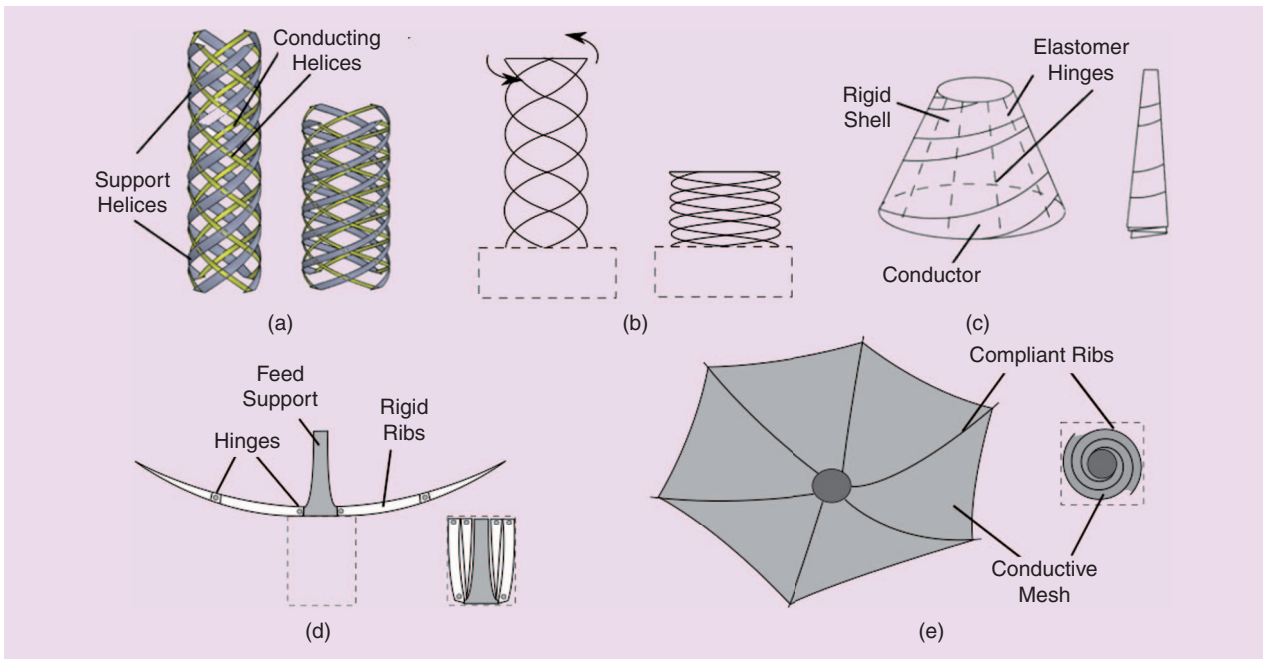


FIGURE 2. Packaging schemes for CubeSat antennas: (a) the helical pantograph, (b) coilable conductors, (c) dual-matrix composite shells, (d) hinged ribs, and (e) the wrapped mesh.

TABLE 1. A SUMMARY OF ANTENNA AND DEPLOYMENT ARCHITECTURES USED IN THE PRESENT STUDY.

	Hinge	Tape-Springs	Helical Pantographs	Z-Folded Shells	Miura–Ori Shells	Coilable Conductors	Hinged Ribs	Wrapped Mesh
Dipole	X	X						
Helix			X	X	X	X		
CLS				X	X			
Horn				X	X			
Patch								
Reflector							X	X
Yagi–Uda		X						

TABLE 2. THE DESIGN EQUATIONS FOR ELECTROMAGNETIC PERFORMANCE METRICS.

Antenna Type	Gain, G	Fractional Bandwidth, BW (%)	Polarization
Half-wavelength dipole	1.643	3	Linear
Single helix	$\frac{15(\pi D)^2 h}{\lambda^3}$	56	Circular
CLS	Interpolated from experimental data in [15]	Interpolated from experimental data in [15]	Circular
Conical horn	$20 \log\left(\frac{\pi D}{\lambda}\right) - \ell$; $\ell = 2.912$ for optimum	$40 < BW < 75$	Linear/circular
Patch	$\frac{2}{15G_{\text{rad}}}\left(\frac{D}{\lambda}\right)^2$	$\frac{\epsilon_r - 1}{\epsilon_r^2} \frac{Dt}{h}$	Linear/circular
Reflector	$\left(\frac{\pi D}{\lambda}\right)^2 \epsilon_{\text{ap}}$	$5 < BW < 10$	Various
Yagi–Uda	Interpolated from experimental data in [20]	Interpolated from experimental data in [20]	Linear

TABLE 3. THE DESIGN EQUATIONS FOR STRUCTURAL PERFORMANCE METRICS.

Antenna Type	Folding Scheme	Packaged Dimensions, L_1, L_2, L_3	Packaging Ratio, ρ	Fundamental Frequency, f_0
Dipole	Hinge	$L_1 = h; L_2 = L_3 = D_{\text{wire}}$	1	$\frac{3.516}{2\pi h^2} \sqrt{\frac{EI}{\rho}}$
	Tape-springs	$L_1 = \frac{h}{i}; L_2 = L_3 = D_{\text{wire}}$		
Helix	Helical pantographs	$L_1 = L_2 =$ $2\sqrt{\left(\frac{D}{2}\right)^2 + \left(\frac{h}{N}\right)^2} - \left(\frac{a}{2\pi}\right)$	$\frac{D^2 h}{2ND_{\text{wire}} L_1}$	$\frac{D_{\text{wire}}}{4\pi D^2 N} \sqrt{\frac{E}{\rho(1+\nu)}}$
		$L_3 = \frac{3}{2} h D_{\text{wire}}$		
	Coilable conductors	$L_1 = 2ND_{\text{wire}}$ $L_2 = L_3 =$ $\frac{1}{\pi} \sqrt{(\pi D)^2 + \left(\frac{h}{N}\right)^2} - 4D_{\text{wire}}^2$	$\frac{D^2 h}{L_1 L_2^2}$	
		Z-folding	$L_1 = h; L_2 = \frac{\pi D}{i}; L_3 = 3ti$	$C_1 D$ $C_1 = 50 \text{ m}^{-1}$
Miura-Ori	$L_1 = L_2 = \frac{\pi D}{2i}; L_3 = \frac{\pi D}{2i} \tan \phi + \frac{h}{j}$			
Conic horn/CLS	Z-folding	$L_1 = g \left[1 + \left(\frac{D \cot \theta}{2h} - 1 \right) \cdot \left(1 - \cos \frac{\theta_0}{2i} \right) \right]$ $L_2 = 2g \frac{D \cot \theta}{2h} \sin \frac{\theta_0}{2i}; L_3 = 3ti$ $g = h \sqrt{\tan^2 \theta + 1}; \theta_0 = \frac{\pi h \tan \theta}{g}$	$C_2 \frac{Dh}{\sqrt{h^2 + \frac{D^2}{4}}}$ $C_2 = 133 \text{ m}^{-1}$	$\frac{2h}{\sqrt{15 \pi D^2}} \left(3 - 4 \sin \left(\frac{3\theta}{4} \right) \right) \sqrt{\frac{E}{\rho(1-\nu^2)}}$ where $\tan \theta = \frac{D}{2h}$
		Miura-Ori	$L_1 = L_2 = \frac{\pi D}{2i}$ $L_3 = \frac{\pi D}{2i} \tan \phi + \frac{1}{j} \sqrt{h^2 + \frac{D^2}{4}}$	
Patch	Fixed	$L_1 = h; L_2 = D; L_3 = t$	1	$\frac{a}{2\pi h^2} \sqrt{\frac{Et^3}{12\rho(1-\nu^2)}}$ $a = f\left(\frac{h}{D}\right)$ can be found in [19]
Reflector	Hinged ribs	$L_1 = L_2 = \frac{D}{10}$ $L_3 = \frac{h}{2} \tan^{-1} \left \frac{\frac{h}{2D}}{\left(\frac{h}{D}\right)^2 - \frac{1}{16}} \right $	$\frac{D^2 h}{L_1^2 L_3}$	$\min \left(\frac{2t^2}{\pi h^3} \sqrt{\frac{E}{\rho}} \frac{g_1}{g_2}, \frac{3}{8\pi} \frac{h}{D_{\text{hub}}} \sqrt{\frac{E}{\rho_{\text{hub}}(1+\nu)}} \right)$ $\frac{g_1}{g_2} = f(\theta_0)$ can be found in [14]
	Wrapped mesh	$L_1 = \frac{\pi D}{i}$ $L_2 = L_3 = D_{\text{hub}} + 3t \cot \frac{\pi}{i}$	$\frac{iDh}{4L_2^2}$	
Yagi-Uda	Tape-springs	$L_1 = D_{\text{wire}}(\pi + 2)$ $L_2 = \frac{\pi}{2} D_{\text{wire}}; L_3 = D_{\text{wire}}$	$\frac{2hD}{D_{\text{wire}}^2(\pi + 2)}$	$\frac{0.621}{h^2} \sqrt{\frac{EtD_{\text{wire}}^3}{\pi\rho}}$

PREDICTING ANTENNA PERFORMANCE

Having parametrized the geometry of the chosen antennas in terms of two common parameters, h and D , the performance of each antenna can be predicted. The electromagnetic performance is characterized by three metrics: maximum antenna gain, fractional bandwidth, and polarization. These metrics can be computed from textbook equations [14] and experimental data [15]. The fractional bandwidth for the horn is derived from the performance range of commercially available antennas.

These results are summarized in Table 2. It is important to note that the electromagnetic performance of the chosen antennas depends also on nongeometric parameters, including material properties, the feeding technique, and various other factors. However, in an initial design, it is acceptable to predict performance based only on geometry; making specific, although preliminary, assumptions about these various effects is sufficient.

The key metric for structural performance of a deployable antenna is its ability to achieve and maintain its deployed configuration, which is best captured by the stiffness of the deployed structure in its softest mode of deformation.

The fundamental frequency of vibration in the deployed configuration captures this effect and is, therefore, a key design metric. Furthermore, the packaging performance associated with a given folding scheme is characterized by the dimensions of the envelope of the folded structure. In addition, a packaging ratio is introduced to measure the ratio of the enclosed volumes in the deployed and folded configurations.

A summary of the equations used to compute the structural performance is presented in Table 3. The fundamental frequency of the vibration of each antenna has been approximated using equations available in [19]. The packaged lengths and packaging ratios have been derived from [13] or computed directly. The structural metrics depend on the geometry as well as material parameters for which specific assumptions are made based on existing antenna prototypes. These include the Young's modulus, E , Poisson's ratio, ν , linear/areal density, ρ , the number of turns in the helix, N , the number of panels in the packaging scheme, i, j , along the axis and the circumference of the antenna, the Miura–Ori panel angle, ϕ , the conductor diameter, D_{wire} , and the central hub diameter, D_{hub} .

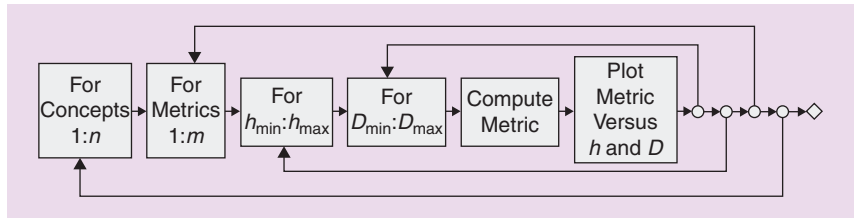


FIGURE 3. The algorithm for estimating antenna performance.

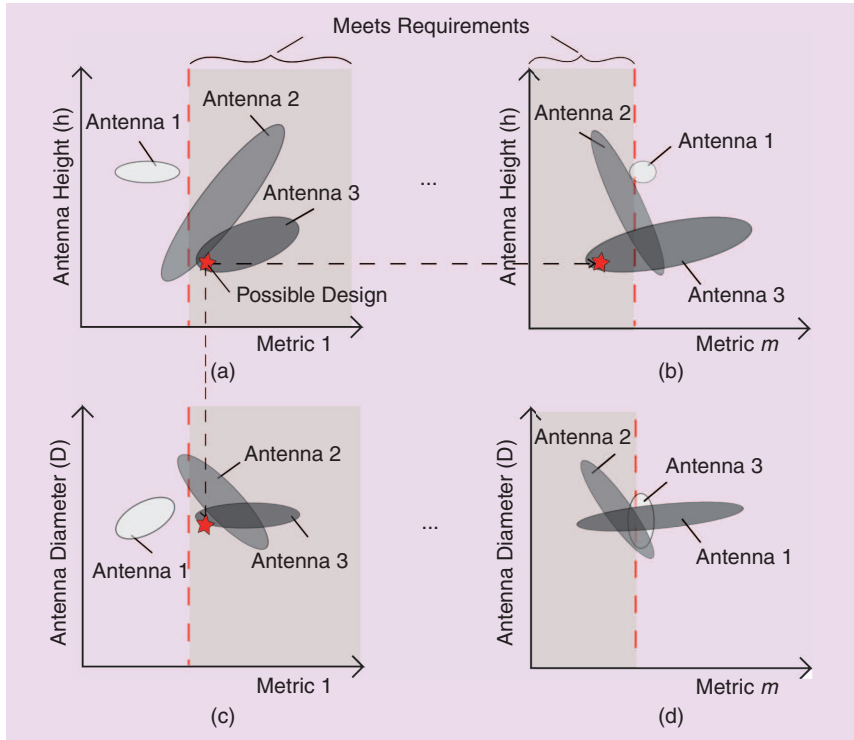


FIGURE 4. (a)–(d) A schematic chart for comparing antenna performance.

PLOTS OF PERFORMANCE METRICS

The design problem is formulated as follows. Given a desired operating frequency for the antenna, one calculates the corresponding wavelength. Then, a set of n antenna concepts is selected, and m performance metrics are computed within four nested loops as a function of h and D , as illustrated in Figure 3. The limits h_{\min} , h_{\max} , D_{\min} , and D_{\max} are computed for each antenna concept using the constraints in the “Antenna Types” section, and the metrics are evaluated using the equations in Tables 2 and 3. Note that this is a brute-force approach, which can be sped up only through coarser discretization of the range of h and D for each antenna. A more efficient algorithm will be developed in the future to accommodate comparisons between a larger number of concepts.

The algorithm in Figure 3 generates the set of plots shown in Figure 4; the layout of which is inspired by Ashby's quad-charts [10]. Figure 4(a) and (b) show the range of each performance metric that can be achieved, for each antenna, by varying the antenna height. Similarly, Figure 4(c) and (d) show the effects of varying the antenna diameter. For each antenna, the locus of performance is shown as an ellipse, although the region may be nonconvex or disjoint.

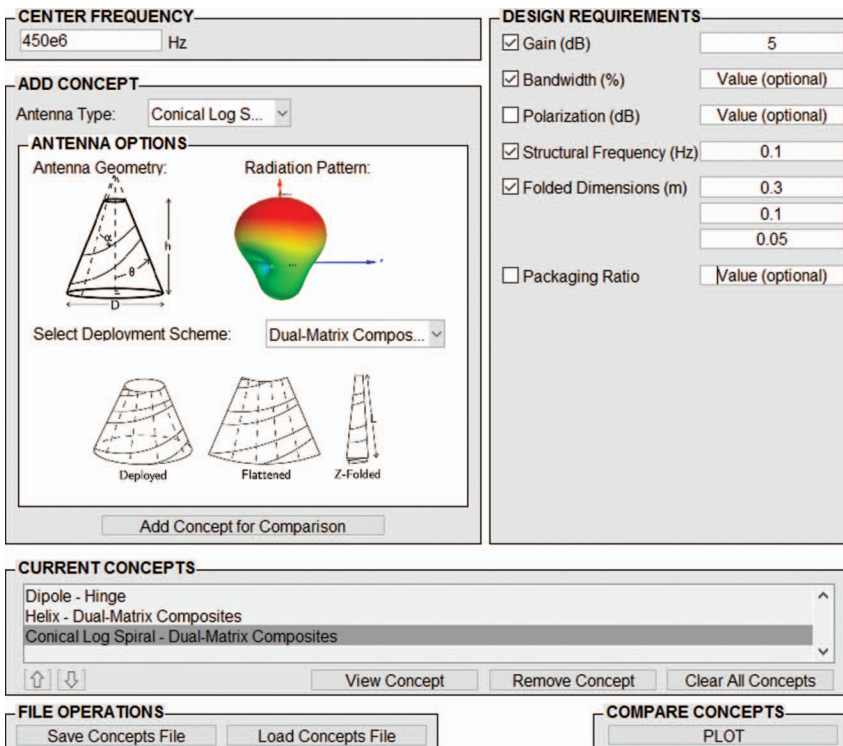


FIGURE 5. The concept selection tool input screen.

Moving across Figure 4, the y -axis value remains constant, whereas moving down, the x -axis remains constant. This allows the tracking of a particular design of a chosen antenna across the whole chart, as illustrated by means of red stars in Figure 4. In each plot, the shaded rectangles identify the region of the antenna performance that satisfies a requirement prescribed for that metric. Those parts of the elliptical loci that lie within the shaded region represent designs that satisfy the requirements for that metric. By looking across several plots, as well as up and down, designers can find subsets of the design space that meet the requirements on all metrics. Therefore, the final result is a set of antenna geometries, parameterized in terms of h and D , that are capable of meeting all requirements. This set can be used for a follow-on, detailed optimization.

TABLE 4. THE DESIGN AND OPTIMIZATION SPACES FOR THE UHF CASE STUDY.

Antenna Architecture	Original Design Space (m)	Optimization Space (m)
Dipole hinge	$h = 0.33$ $D = 0.025$	Does not meet requirements
Single helix Z-folding	$0.012 < h < 3.32$ $D = 0.21$	$0.22 < h < 0.27$ $D = 0.21$
Conical horn Z-folding	$1.73 < h < 65.53$ $2.00 < D < 11.47$	Does not meet requirements
CLS Z-folding	$0.21 < h < 23.40$ $0.13 < D < 2.27$	$0.21 < h < 0.27$ $0.20 < D < 0.30$

PRELIMINARY DESIGN TOOL

A design interface is developed to implement the suggested methodology in MATLAB. The tool allows one to enter the requirements for the design problem and the antenna concepts to be compared, as shown in Figure 5. The user can compare different antenna types or a single antenna packaged using several schemes, for an arbitrary number of parameters. The tool allows designers to select and compare various antenna topologies against multiple deployment approaches before selecting an optimal solution that will then be modeled using any of the numerical simulators available for detailed radiation characteristic and electromagnetic performance evaluation. As a result, the tool reduces the selection and comparison time in the preliminary design stages.

UHF ANTENNA DESIGN CASE STUDY

A case study of a UHF antenna operating at 450 MHz is presented to demonstrate the methodology. The antenna

concepts compared are 1) a dipole packaged using a mechanical hinge and 2) a helix, CLS, and horn all packaged using Z-folding. The following requirements are prescribed on the design: a gain in excess of 5 dB, a fundamental structural frequency higher than 0.1 Hz, a packaged antenna fitting in a $(1/2)$ 3U CubeSat ($30 \times 10 \times 5$ cm³ volume), and a maximum bandwidth.

The requirements define a coupled electromagnetic and structural design problem appropriate for the aforementioned methodology. The geometric constraints on the height and diameter are calculated from (1), (3), (4), and (6), respectively, for the four antennas and are given in the second column of Table 4. The gain, fractional bandwidth, fundamental frequency, and packaged dimensions are computed from the equations in Tables 2 and 3, for the full range of geometric parameters. These metrics are plotted against the antenna geometry as described in the "Plots of Performance Metrics" section, and the result is shown in Figure 6.

To select specific antenna architectures that meet all the requirements, start from Figure 6(a). This plot identifies designs meeting the gain requirement; therefore, the region with gain higher than 5 dB (3.16 dimensionless) is shaded gray in the plot. The locus for the dipole antenna (which is a single point) falls outside the shaded area, indicating that it does not meet the gain requirement. Note also that the entire locus for the conical horn antenna falls inside the shaded area, showing that it meets the gain requirement. Regarding the loci for the single helix and the CLS, only subsets fall within the shaded area. The height ranges corresponding to these subsets identify viable CLS antennas, with any height, and helical antennas with $0.22 < h < 3.32$ m.

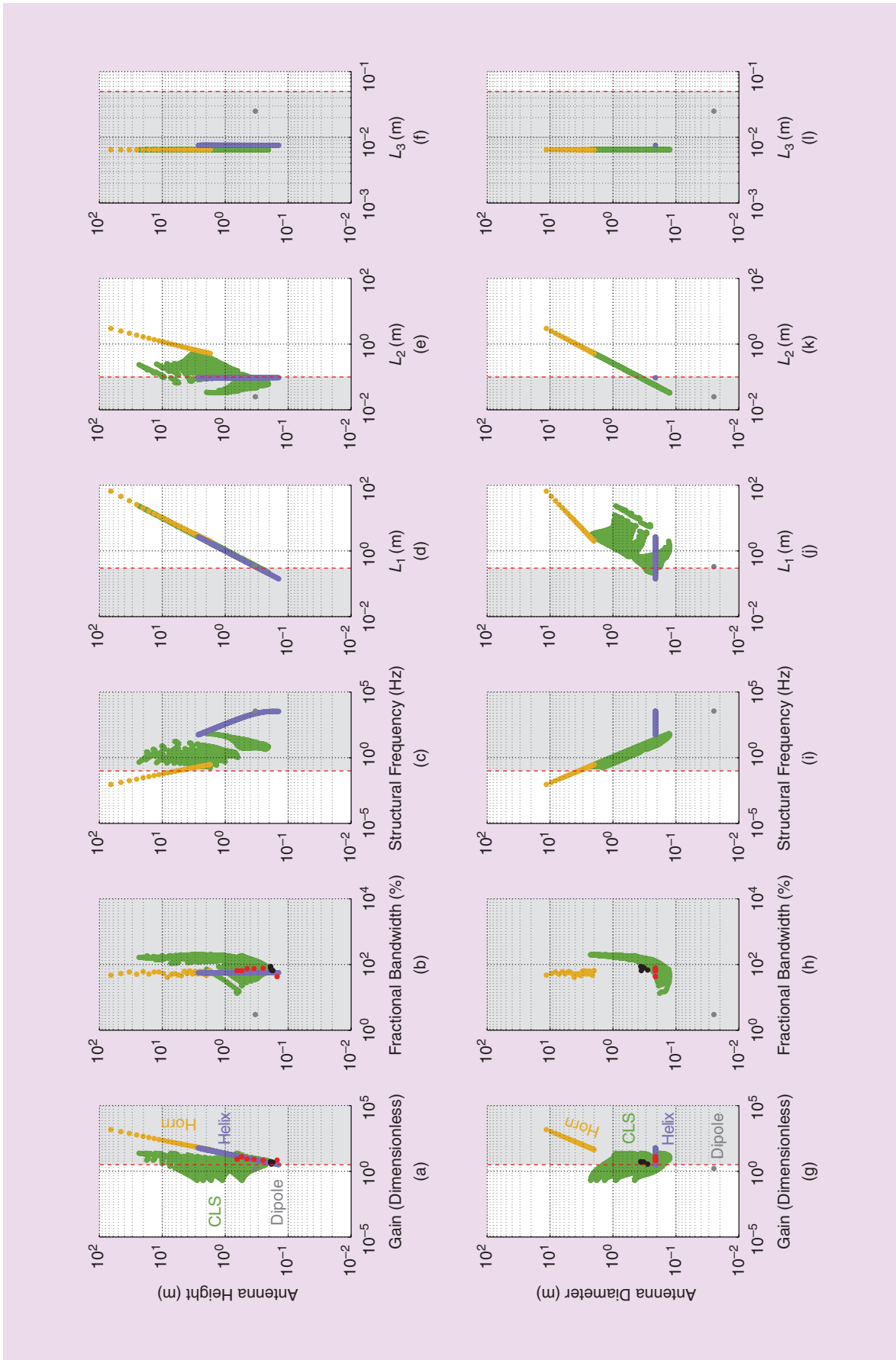


FIGURE 6. (a)–(l) The concept selection chart for the design of a high-performance UHF antenna operating at 450 MHz that folds in half of a 3U CubeSat. The red and black dots indicate helix and CLS antennas, respectively, designed using numerical simulations.

Moving to the right from Figure 6(a), the same process can be repeated for plots in Figure 6(b)–(f). Figure 6(b) imposes no new constraints on the design as no requirement is specified for the bandwidth. However, it can be seen that the CLS maximizes the fractional bandwidth. In Figure 6(c), it is found that only conical horn antenna heights in the range $1.4 < h < 3.2$ m meet the structural frequency requirement, whereas there is no limitation on the helical and CLS antennas. Proceeding to Figure 6(d), introducing a constraint on the largest packaged length of 0.3 m, eliminates the conical horn antenna (indicating that the chosen packaging scheme is not acceptable). Of the remaining two viable concepts, the characteristic length requirement is met by helical antennas with $0.012 < h < 0.27$ m and CLS antennas with $0.21 < h < 0.27$ m. Similarly, Figure 6(e) imposes that $0.21 < h < 10.0$ m for the CLS. No additional constraints are given by Figure 6(f).

The analysis of the first row of plots in Figure 6 has led to the conclusion that the dipole and conical horn cannot meet all the requirements. At this point, an analysis similar to that described previously, but using Figure 6(g)–(l), provides the range of viable diameters for the helix and CLS. The outcome of the analysis is the h and D ranges meeting all requirements presented in the third column of Table 4. At this point, detailed simulations can be carried out to complete the design optimization.

Antenna designs generated independently via numerical simulations in ANSYS HFSS for this case study are denoted by red and black markers in Figure 6 for the helix and CLS antennas, respectively. A good agreement is seen between these and the designs that are presented by the methodology here.

CONCLUSIONS

A methodology for the rapid preliminary design of deployable antennas for CubeSats is proposed. Using a novel visual representation method of antenna performance consisting of a coordinated set of plots of antenna performance metrics against the antenna geometric parameters, it can easily address coupled electromagnetic and structural design problems. This approach enables a direct comparison of antenna concepts and allows the designer to rapidly identify concepts that meet requirements and to narrow down the design space before tackling the problem with detailed numerical simulations.

The design of a UHF antenna operating at 450 MHz is used to demonstrate the method. The technique eliminates antenna designs unable to meet requirements, which achieves a reduction of the original design space by several orders of magnitude. The results agree well with the antenna designs optimized using numerical simulations.

The methodology is demonstrated using a relatively small number of antenna types, packaging schemes, and performance metrics. However, the method itself is quite general and can be extended further. For example, an antenna mass performance metric and material selection can be incorporated in the tool. The software tool that has been developed could also be combined with existing databases of antenna and structural performances to provide rapid designs over much larger design spaces.

ACKNOWLEDGMENTS

This research was supported by the Air Force Office of Scientific Research (award no. FA9550-13-1-0061).

AUTHOR INFORMATION

M. Sakovsky (msakovsk@caltech.edu) is with the Graduate Aerospace Laboratories at the California Institute of Technology, Pasadena. Her research interests lie in deployable composite structures for space applications.

S. Pellegrino (sergiop@caltech.edu) is with the Graduate Aerospace Laboratories at the California Institute of Technology, Pasadena. His current research interests include the mechanics of lightweight structures, with a focus on packaging, deployment, shape control, and stability.

J. Costantine (jcostantine@ieee.org) is with the Electrical and Computer Engineering Department, American University of Beirut, Lebanon, and also with COSMIAC, Albuquerque, New Mexico. His major research interests are in reconfigurable antennas for wireless communication systems, cognitive radio, antennas for biomedical applications, and deployable antennas for small satellites.

REFERENCES

- [1] Helios Communication Technologies. Helios deployable antenna. [Online]. Available: <http://www.helicomtech.com/helios-deployable-series>
- [2] J. Sauder, N. Chahat, M. Thomson, R. Hodges, and Y. Rahmat-Samii, "Ultra-compact ka-band parabolic deployable antenna for CubeSats," presented at Interplanetary CubeSat Workshop, Pasadena, CA, 2014.
- [3] C. S. MacGillivray, "Miniature deployable high gain antenna for CubeSats," presented at 8th CubeSat Developers Workshop, San Luis Obispo, CA, 2011.
- [4] P. Muri, O. Challa, and J. McNair, "Enhancing small satellite communication through effective antenna system design," in *Proc. Military Communications Conf.*, San Jose, CA, 2010, pp. 347–352.
- [5] ANSYS. ANSYS HFSS Simulation Software. [Online]. Available: www.ansys.com/Products/Electronics/ANSYS-HFSS
- [6] CST. Computer Simulation Technology Software. [Online]. Available: www.cst.com
- [7] Altrait Engineering. FEKO. [Online]. Available: www.feko.info
- [8] Antenna Magus. [Online]. Available: <http://www.antennamagus.com/>
- [9] Dassault Systèmes. Abaqus. [Online]. Available: www.3ds.com/products-services/simulia/products/abaqus/
- [10] M. F. Ashby, *Materials Selection in Mechanical Design*, 3rd ed. Oxford: Elsevier, 2005.
- [11] Granta. *CES Selector*. [Online]. Available: www.grantadesign.com/products/ces/
- [12] M. Sakovsky, I. Maqueda, C. Karl, S. Pellegrino, and J. Costantine, "Dual-matrix composite wideband antenna structures for CubeSats," presented at AIAA Spacecraft Structures Conf., Kissimmee, FL, 2015.
- [13] G. M. Olson, S. Pellegrino, J. Banik, and J. Costantine, "Deployable helical antennas for CubeSats," presented at 54th AIAA/ASME/ASCE/AHS/ASC Structures, Structural Dynamics, and Materials Conf., Boston, MA, 2013.
- [14] C. A. Balanis, *Antenna Theory: Analysis and Design*, 4th ed. Hoboken, NJ: Wiley, 2016.
- [15] J. D. Dyson, "The characteristics and design of the conical log-spiral antenna," *IEEE Trans. Antennas Propag.*, vol. 13, no. 4, pp. 488–499, 1965.
- [16] J. Costantine, Y. Tawk, C. G. Christodoulou, J. Banik, and S. Lane, "Cube-Sat deployable antenna using bistable composite tape-springs," *IEEE Antennas Wireless Propag. Lett.*, vol. 11, pp. 285–288, Feb. 2012.
- [17] L. K. Alminde, K. Kaas, M. Bisgaard, J. Christiansen, and D. Gerhardt, "GOMX-1 flight experience and air traffic monitoring results," presented at 28th Annu. AIAA/USU Conf. Small Satellites, Logan, UT, 2014.
- [18] T. Murphey, S. Jeon, A. Biskner, and G. Sanford, "Deployable booms and antennas using bi-stable tape-springs," presented at 24th Annu. AIAA/USU Conf. Small Satellites, Logan, UT, 2010.
- [19] R. D. Blevins, *Formulas for Natural Frequency and Mode Shapes*, 1st ed. New York: Litton Educational Publishing, 1979.
- [20] P. P. Viezbicke, "Yagi Antenna Design," National Bureau of Standards, Gaithersburg, MD, Tech. Note 688, 1968.

